Journal of Energy Storage 50 (2022) 104144

Contents lists available at ScienceDirect

Journal of Energy Storage

journal homepage: www.elsevier.com/locate/est

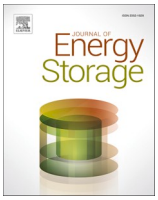

Research Papers

Early Quality Classification and Prediction of Battery Cycle Life in Production Using Machine Learning

Sandro Stock *, Sebastian Pohlmann, Florian J. Günter, Lucas Hille, Jan Hagemeister, Gunther Reinhart

Institute for Machine Tools and Industrial Management, Technical University of Munich, Boltzmannstr. 15, Garching 85748, Germany

A B S T R A C T

An accurate determination of the product quality is one of the key challenges in lithium-ion battery (LIB) production. Since LIBs are complex, electrochemical systems, conventional quality control measures such as aging are time-intensive and costly. This paper presents the applicability of machine learning approaches for an early quality prediction and a classification of cells in production. Using inline measurement data of 29 NMC111/graphite pouch cells, linear regression models and artificial neural networks (ANNs) were compared regarding their prediction accuracy. From comprehensive electrochemical impedance spectroscopy (EIS) and cycling datasets, a total of 24 features were extracted, combined, and analyzed. The best ANN achieved a test error of 10.1% at an observation time of less than two days. For a classification into two cycle life groups, a maximum accuracy of 97% was reached. Moreover, a reliable classification of high-lifetime cells was achieved using only EIS measurements during wetting. The results highlight the great potential of data-driven models for the prediction of LIB quality in production as well as their implementation to increase the throughput and the overall cell quality.

1. Introduction

Reducing greenhouse gas emissions is one of the biggest current challenges for society, leading manufacturers to push the development of electric vehicles (EVs). For powering EVs, lithium-ion batteries (LIBs) as electrochemical storage devices have taken a predominant role due to their high energy density as well as their long cyclical and calendrical lifetime [1]. So far, high costs and safety concerns have limited broad market penetration. Increasing quality and reducing manufacturing costs within the battery production is therefore a key challenge [2].

Looking at the production chain, battery quality is primarily examined in the final process steps: formation, aging, and end-of-line (EoL)-testing [2]. These steps are critical for ensuring high-quality LIBs but add a great expense to the manufacturing costs [3]. During the formation, the cell capacity is determined as the first indicator for the overall cell quality [4]. From the cell capacity, only major errors in production can be derived and no information about the expected cycle life is provided [5]. As LIBs must fulfill highest safety standards during several years of operations, the quality of the cells is determined in a time-consuming aging process [6]. During aging, cells are stored in climate chambers and monitored using battery test systems. A self-discharge of the LIBs during storage is observable, which generates a leakage current. The resulting leakage current is defined as the internal current after completion of the post-charge diffusion [7]. The leakage current is measured continuously and is usually used as an indicator for the quality of the cells. Defect cells are detectable by an increased leakage current and are removed in the subsequent EoL-test. However, the leakage current decreases non-linearly and converges below a critical threshold value after sufficient measuring time [8]. Therefore, a measuring time of up to 3 weeks is necessary for quality assurance [9]. With 28.7% of the total manufacturing costs, formation and aging account for a considerable share [10]. One feasible approach is the use of predictive quality models to identify the cell quality before entering the aging step to reduce the process time or even eliminate the entire process step. Hence, methods for the early prediction of battery life based on production data are required.

In recent years, several data-driven methods were proposed to analyze the state and quality of LIBs using a wide range of analysis methods [11]. To predict the lifetime or the remaining useful life (RUL), a variety of methods from the fields of stochastic processes, filtering, and artificial methods were applied [12]. In particular, feature-based approaches are a promising solution [13]. For these approaches, cell data is collected using battery test systems, and suitable features are identified and selected [14]. Based on these, machine learning models were developed and applied to determine correlations in the datasets [15]. The aim is to obtain a high correlation between features of the dataset and the lifetime of the cell [16].

The end of the cell lifetime is commonly defined at 80% of the initial

* Corresponding author.
E-mail address: sandro.stock@iwb.tum.de (S. Stock).

https://doi.org/10.1016/j.est.2022.104144
Received 11 July 2021; Received in revised form 12 January 2022; Accepted 30 January 2022
Available online 20 February 2022

capacity [17]. The corresponding number of cycles (charging and discharging process) at which the final capacity is reached, is defined as the cycle life of the cell. Due to the increasing computing power, much effort is spent lately on the development of prediction models using machine learning and artificial intelligence approaches.

Among the first, Wu et al. showed that an online RUL estimation is possible using a feed-forward neural network. They achieved an error of less than 5% in cycle life prediction within practical operation but were using the cycling data of two LIBs only [18]. Mansouri et al. examined the RUL of lithium polymer batteries based on voltage data analysis. By comparing linear and non-linear models, they concluded that non-linear models outperform linear models, even with optimization methods such as the "least absolute shrinkage and selection operator" (LASSO) [19]. Ren et al. achieved the best accuracy rate of 88.2% for RUL prediction with 21 extracted features and a deep neural network in comparison to linear regression, a Bayesian regression, and a support vector machine (SVM), and a high number of input cycles [20]. Besides the prediction of the RUL, the early classification of LIBs into high and low lifetime groups was investigated. Zhu et al. 2019 compared machine learning models like decision trees, SVM, and k-nearest-neighbor based on the accuracy of the lifetime prediction [21]. They achieved the highest accuracy of 95.2% classifying commercial iron phosphate (LFP)/graphite LIBs in two groups with a threshold at 550 cycles using a decision tree model. Furthermore, the capacity difference between the initial two cycles was identified as the most important feature for the prediction. Tracing back the strongly fluctuating lifetime of the tested cells was not possible, since no information on production and material properties was given. Severson et al. also classified commercial LFP/graphite LIBs at a threshold of 550 cycles using the features extracted from five input cycles. Using a logistic regression model and nine features, they achieved a test error of 4.9% [22]. In addition, a cycle life prediction was performed with a linear regression model, achieving a test error of 9.1% with a very high number of 100 input cycles.

The variety of battery cell systems and applied machine learning methods demonstrate the power of RUL prediction and cycle life classification in LIB quality analysis. However, these models were applied to commercial cells only. Defective and short-lifetime cells were detected exclusively during the operation. This is highly problematic since LIBs are usually packaged or assembled into battery packs after production and defective cells cannot be removed despite accurate prediction. Therefore, a method for an early quality prediction during production is required to detect production errors before the cells are further processed.

In this work, machine learning approaches were examined and used to predict cell cycle life using data from wetting, formation, and early cycling without the need for complex degradation models. In-house manufactured pouch cells with varied electrolyte quantities were evaluated concerning the achievable cycle life. Since promising results in predicting cycle life were obtained in the literature with both an ANN and a linear regression model, both methods were examined and compared using a total of 24 input features. The most suitable model was chosen for quality classification as well as the prediction performance evaluation. Subsequently, a classification in groups with low and high cycle life was performed using data from the production processes and early cycling. The prediction and classification models were combined to generate a grading into four quality groups. Finally, production strategies are presented based on the prediction models to increase the throughput and enhance the overall quality.

2. Experimental

The large-format multilayer pouch cells used in this work were assembled on the semiautomatic manufacturing pilot line at the Technical University of Munich [23]. For the production of the LIBs, commercially available double-sided coated cathode and anode coils were purchased. Detailed information on the electrode specifications and production are provided by Günter et al. [24]. The essential aspects are briefly summarized in the following.

2.1. Cell assembly

Cell assembly was performed inside a dry room with a dew point of less than -45 °C. Electrode roll material was separated using a laser cutting process with an automated material feed and a cutting speed of 0.8 m/s. Anodes were cut to a format of 101 mm x 73 mm and cathodes to a format of 104 mm x 76 mm. The sheets were stacked by an automated z-folding system with a commercial membrane separator (Celgard 2325) in between the electrodes. Each cell stack contained 13 anode sheets and 12 cathode sheets. The current collector foils and the cell tabs were joined by ultrasonic welding (Branson Ultraweld L20). The welded cell stacks were packaged into a flexible, deep-drawn pouch bag foil and subsequently sealed at three sides. To ensure that the ppm of water molecules decreases sufficiently prior to the electrolyte filling, the packaged cell stacks were dried in a vacuum oven at 60 °C and 20 mbar in three repeating cycles.

2.2. Electrolyte filling

The electrolyte (LP572, BASF) consisted of 1 M $LiPF_6$ in a mixture of ethylene carbonate (EC) and ethyl methyl carbonate (EMC) at a weight ratio of 3:7 for EC:EMC with 2 wt% vinylene carbonate (VC). The pouch cells were filled with a single dosing step since the amount of electrolyte can fit in the entire void volume of the cell. Before dosing, the filling chamber was flushed with nitrogen to reduce the ambient water concentration. Subsequently, the electrolyte was injected with a pressure of 80 mbar. The electrolyte quantity was intentionally varied to simulate process deviations. The number of cells per dosing volume with the respective electrolyte quantity are summarized in Table 1. The cells were subsequently sealed and positioned horizontally for the 180 min wetting procedure.

2.3. Formation

A battery cell test system (CTS, BaSyTec) was used for the formation of the cells. The temperatures, the voltages, and the currents were tracked with the corresponding BaSyTec software. The cell capacities were determined by the last discharge cycle during formation and are shown in Table 1. Table 2 shows the formation protocol. During SEI formation, gasses are produced which are directed into the gas bag by applying external pressure to the cell. This was achieved by a specially designed cell fixture that applies a constant mechanical pressure of 0.2 MPa on the cell. After formation, the cells were degassed and subsequently sealed. Degassing was done inside a nitrogen-flushed vacuum chamber at an evacuated pressure of 100 mbar.

2.4. Cycle life testing

Cycle life testing was performed inside a controlled climate chamber at a temperature of 25 °C using the same cell fixture for pressure application as in the formation process. Table 2 shows the cycling protocol that contains 50 cycles at 1C with two recovery cycles at C/10 and C/2, respectively. Recovery cycles are implemented to determine the irreversible capacity loss. Fig. 1 shows the discharge capacity of the 1C cycles during cycle life testing. The course of the discharge capacity for increasing cycle numbers is displayed until the end-of-life capacity is reached. End-of-life capacity is defined at 80% of the initial capacity [17]. The corresponding number of cycles at which the end-of-life capacity is reached is defined as the cycle life of the cell. Each cell is color-coded according to the respective cycle life. The inset displays the first 20 cycles, which are used as input data for the later prediction and classification. The strong variation in the cycle life can be attributed to variations in the electrolyte quantity. Depending on the electrolyte

Table 1
Controlled variation of the electrolyte quantity to simulate production errors and to obtain deviations in the cycle life. The values in the parentheses for the "number of cells" corresponds to the number of cells that were rebuilt in a second batch. The cell capacity was determined at 25 °C and the last formation cycle at a discharge current of 0.486 A.

Number of cells	3	3	3	6 (3)	3	7 (4)	4 (4)
Electrolyte quantity	(7.11±0.05) ml	(8.70±0.17) ml	(10.98±0.05) ml	(12.38±0.33) ml	(14.26±0.19) ml	(15.83±0.26) ml	(19.62±0.53) ml
Cell capacity	(3.28±0.04) Ah	(3.31±0.03) Ah	(3.05±0.23) Ah	(3.32±0.11) Ah	(3.41±0.02) Ah	(3.42±0.03) Ah	(3.46±0.02) Ah

Table 2
Measurement procedures applied to the pouch cells. All procedures were performed in a controlled climate chamber at a temperature of 25 °C. During formation, the current was identical for all cells, whereas during cycling, the C-rate was determined based on the cell capacity after formation. Data points were recorded every 10 s. Abbreviations–CC–Constant current, CV – Constant voltage, $U_{max} = 4.2$ V, $U_{min} = 2.7$ V.

Procedure	Direction	(Dis)charge	Stop condition	Cycles	Loops
Formation	charge	CC @ 0.486 A	$U > U_{max}$		
	charge	CV @ U_{max}	$I < 0.243$ A	2	1
	discharge	CC @ 0.486 A	$U < U_{min}$		
Cycling	charge	CC @ C/10	$U > U_{max}$		
	charge	CV @ U_{max}	$I < C/20$	1	
	discharge	CC @ C/10	$U < U_{min}$		
	charge	CC @ C/2	$U > U_{max}$		
	charge	CV @ U_{max}	$I < C/20$	1	20
	discharge	CC @ C/2	$U < U_{min}$		
	charge	CC @ 1C	$U > U_{max}$		
	charge	CV @ U_{max}	$I < C/20$	50	
	discharge	CC @ 1C	$U < U_{min}$		

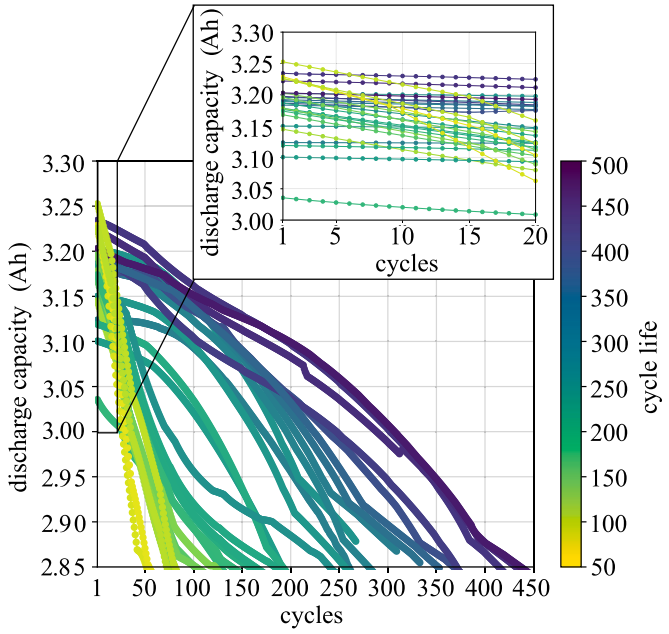

Fig. 1. Capacity degradation of the examined cells. The figure shows the discharge capacity over sequential cycles for 29 NMC111/graphite pouch cells at 1C. The C-rate was calculated using the discharge capacity after formation, shown in Table 1. Each data line represents one cell and is color-coded according to the cycle life of the cell. Cycle life is defined as the cycle number in which the capacity drops below 80% of the initial capacity. The inset displays the first 20 cycles which are examined in detail in the paper. The strong variation in the cycle life is due to variations in the electrolyte quantity to introduce process deviations.

quantity, the discharge capacity decreases at different rates and in a different progression. In the first 20 cycles, however, a trend is only evident for the cells with very short cycle lives. A detailed analysis on the dependency of the cycle life on the electrolyte quantity is provided by Günter et al. and addressed in detail in Section 4.2 [24]. The exact cycle life and electrolyte quantity for each cell is shown in the Supplementary Table A1.

2.5. Electrochemical impedance spectroscopy

During wetting, after formation, and after degassing, electrochemical impedance spectroscopy (EIS) measurements were performed using a potentiostat (Interface 5000E, Gamry Instruments). At first, the open-circuit voltage (OCV) was measured for 15 s at a sample period of 0.5 s. The subsequent EIS measurements had a frequency range from 100 kHz to 1 Hz and an alternating current excitation signal amplitude of 10 mV (root mean square) around the OCV. Ten equally distributed sample points were taken per decade and the alternating current was summed with the direct current for the analysis. During wetting, alternating OCV and EIS measurements were repeated for at least 90 min as the wetting state influences the cell impedance [25]. After formation and after degassing, three subsequent measurement cycles were carried out since the cells were in a relatively stable state [24]. The results from the EIS measurement were analyzed using two different approaches. In the classification model, the data was processed unfiltered (see Section 4.3). For the regression model, critical parameters such as the high-frequency resistance (HFR) and low-frequency resistance (LFR) were derived. The HFR is defined as the impedance value at which the imaginary part is zero [25]. The LFR is obtained by linear extrapolation of the low-frequency region in the Nyquist plot, referred to as Warburg impedance [26]. The real part of the impedance of the linear fit at a zero imaginary part gives the value for the LFR (see the Supplementary Figure A2 for further details).

3. Methods

In the methods section, the theory for understanding the prediction and classification models is presented, and the exact specifications explained to ensure easy transferability of the models to production. The production and testing data were first pre-processed to determine relevant parameters, which served as input data for the prediction and classification models. Subsequently, the linear regression model and the artificial neural network were created, and the individual specifications defined.

3.1. Data pre-processing

Linear and non-linear machine learning models were created to predict the cycle life and to classify the LIBs in groups with varying cycle lives. In total, the datasets of 29 pouch cells were recorded and analyzed by machine learning models. The cells were randomly divided into training and test cells with a training-test ratio of approx. 70% to 30%, as suggested by Bhagwat et al. [27]. Of the 29 available cells, 20 cells were used for the training and 9 cells for the test of the models. Three different data sources were used, derived from measurements during wetting, formation, and subsequent cycling. At first, the datasets were pre-processed, and features were created. For each feature, the

Pearson's ratio, also known as the correlation coefficient cor(x, y), were calculated [28]:

$$cor(x,y) = \frac{\sum_{i=1}^{n}(x_i - \bar{x})(y_i - \bar{y})}{\sqrt{\sum_{i=1}^{n}(x_i - \bar{x})^2}\sqrt{\sum_{i=1}^{n}(y_i - \bar{y})^2}} \quad (1)$$

The correlation coefficient is restricted to values between -1 and 1, depending on a positive or negative correlation between two variables x and y. A value higher than |0.8| indicates a high correlation and a value below |0.5| shows a very weak correlation. In between a value of |0.5| and |0.8|, the correlation is moderate [21]. A horizontal bar above the variable denotes the arithmetic mean and the index *i* indicates the summation index. The features were then classified by their correlation and combined for better results. The features and the corresponding correlation coefficients are shown in the Supplementary Table A2. In addition to the feature extraction, a raw data approach was conducted in the classification. In this approach, the complete impedance spectroscopy dataset was provided unfiltered as an input feature set to the model. However, a larger feature set does not necessarily result in a better prediction due to the high dimensionality of the cell data. Especially with a limited data set, there is a risk of reducing the accuracy of the models, since correlations are more difficult to detect [29]. To avoid this issue, the raw data approach was only applied to the EIS and the formation data, because the dimensionality is much lower than in the cycle life data.

3.2. Linear regression model

The features were used as input for a linear regression model. A linear relationship between the feature values x_i and the predicted cycle lives y* is defined according to Eq. (2). Following the approach of Joshi et al., weight parameters w_0 and w_i were introduced to assign different weights to the features [30].

$$y^* = w_0 + \sum_{i=1}^{n} w_i x_i \quad (2)$$

To avoid overfitting, a regularization technique was applied [30]. As a regularization method, the elastic net was used, because of its improved performance when high correlations between features are present [31]. Furthermore, the elastic net shows better performance when analyzing correlations with a higher number of predictors x_i than observations y [32]. The elastic net is a combination of the LASSO regression and the ridge regression. Detailed information on regularized linear regressions is provided by Joshi et al [30]. The resulting loss function for the linear regression is shown in Eq. (3) [33].

$$J(w) = \frac{1}{2n}\sum_{i=1}^{n}\left(y^*(x_{ij}) - y_i\right)^2 + \left(r\lambda\sum_{j=1}^{p}|w_j|\right) + \left(\frac{1-r}{2}\lambda\sum_{j=1}^{p}w_j^2\right) \quad (3)$$

The loss function consists of three terms. The first term is the square error between the predicted cycle life y* and the observed cycle life y. The second and third terms consist of the L1-penalty ($\sum_{j=1}^{p}|w_j|$) and the L2-penalty ($\sum_{j=1}^{p}w_j^2$), respectively. By using the L1-penalty, the absolute value of the weight is added as a penalty term. The L1-penalty uses the squared value of the weight. For the combination between the L1-penalty and the L2-penalty, an additional parameter r and a hyperparameter λ is required. In machine learning, a hyperparameter is defined as a parameter whose value is used to control the learning process [30]. To determine the optimal values for the hyperparameters r and λ, a 4-fold-cross-validation was applied, for which the training data was subdivided into four equal-sized groups, as addressed by Zhang et al. [34]. One group acted as the validation set and the other groups as training data. While varying the hyperparameters, the validation error was analyzed. The optimal values for minimizing the loss function and thereby the model error were determined.

3.3. Artificial neural network

Besides the linear regression model, ANNs were created to solve the regression and the classification problem. The main difference between a regression and a classification is the output. By solving a regression problem, the aim is to predict a continuous variable, e.g. the cycle life. A classification pursues the aim to allocate data to different groups. Since the cells were categorized in distinct groups with different cycle lives the variable was discrete.

ANNs are based on the structure of neural networks in a biological brain. Therefore, artificial neurons are arranged in different layers and connected to each other [35]. An ANN consists of at least one input and one output layer [36]. The layers in between are called hidden layers and any number of hidden layers is possible in general. Using a feed-forward ANN, the information is transported from the input to the output layer. The algorithm which processes the information is a chain of different mathematical functions. At first, the input values in a neuron are summed up. The sum is used in an activation function, where the output of the neuron is calculated [30]. For the later classification task, the cells were divided into different cycle life groups. Thereby, the one-hot encoded representation was used for the different groups. One-hot defines the conversion to a vector with the elements 0 and 1. The value 1 represents the related category and 0 the other vector entries [30]. Thus, the number of elements equals the number of categories. As a loss function for the regression, the mean squared error was used. For the classification, the categorical cross-entropy function L was applied [37]:

$$L(y^*, y) = -\sum_i y_i \log\left(y_i^*\right) \quad (4)$$

It measures the dissimilarity between the observed values y and the predicted values y* [37]. The significance of the models was evaluated by the percentage error, which is defined in Eq. 5:

$$error = \frac{1}{n}\sum_{i=1}^{n}\frac{\left|y_i - y_i^*\right|}{y_i}\cdot 100 \quad (5)$$

3.3.1. Network architecture

Fig. 2 shows the used ANN with five hidden layers. As the input and the output layer vary between the models, they are highlighted in blue. Existing ANNs for the battery cycle life prediction exhibit a simple network architecture with a small amount of hidden layers [38,39]. To determine a suitable network architecture, different feed-forward neural networks were created and compared based on their performance. Fig. 3 presents an extract with the comparison of five network architectures for the classification problem. The structure of the ANNs is shown in Table 3. The loss function decreased strongly during the first epochs for all network configurations considered. The number of epochs defines the repetitions in which the learning algorithm runs through the entire training dataset. An increase in the loss function or strong fluctuations indicated inadequate network (net) structures for network 3 as well as network 1 and network 5. The best results were obtained with the ANN consisting of five hidden layers, while network 4 with two hidden layers showed the lowest fluctuations. Nevertheless, network 2 converged to the lowest value at slightly higher fluctuations. Therefore, network 2 with five hidden layers was selected. Starting in the first hidden layer, the number of neurons was 40, 32, 24, 16, and 8. The results of the comparison of the same network architectures for the regression problem are shown in the Supplementary Fig. 1.

3.3.2. Activation function

The rectified linear unit (RELU) function, shown in Eq. (6), was used as the activation function for all hidden layers [40].

$$\theta(x) = \begin{cases} 0, & for\ x \le 0 \\ x, & for\ x > 0 \end{cases} \quad (6)$$

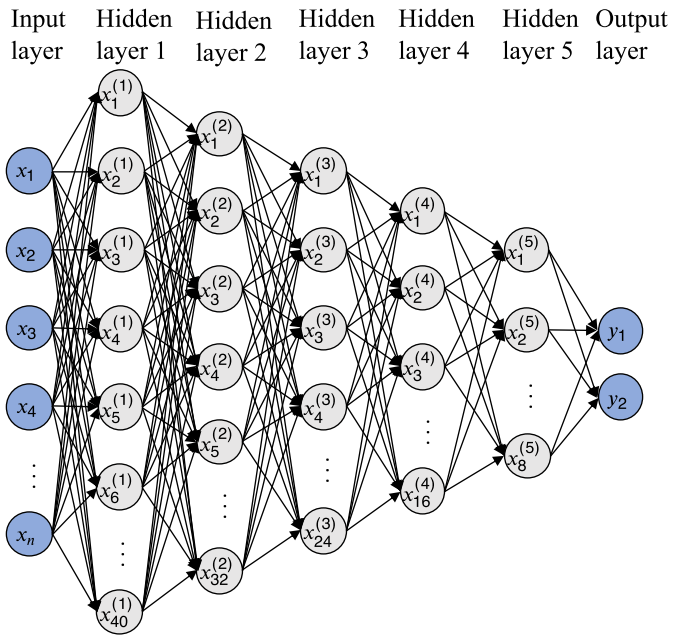

Fig. 2. Representation of the used ANNs. x_i represents the extracted features, $x_n^{(h)}$ the neurons and y_j the output values. Input and output layer are highlighted in blue. The number of hidden layers and respective neurons were constant for both the regression and the classification task. A detailed investigation on the structure of the hidden layers is provided in Fig 3.

Advantages of the RELU-function are efficiency in terms of computation power and a faster convergence than other activation functions [41]. This results in a reduced training time. The activation function for the output layer of the regression problem was the linear function and the Softmax-function for the classification problem. Other frequently used activation functions like the Leaky RELU-function and Maxout were used but showed no improved results.

3.3.3. Optimizer

An optimization algorithm (optimizer) was used to improve the training speed and ensure the accuracy of the results [42]. The AdaMax algorithm was used as an optimizer, since it showed the best performance in comparison to other optimizers, like Adam, AdaGrad, and stochastic gradient descent (SGD). The AdaMax is a variant of the Adam optimizer and is based on the infinity norm [43].

3.3.4. Learning rate

An adaptive learning rate is used for the model to adjust the step size at each iteration when approaching the minimum of the loss function [30]. Hence, the model can react to an increasing loss function by decreasing the learning rate, which reduces the error. A value of 0.1 for the adaptive learning rate was identified as suitable.

3.3.5. Regularization method

To reduce overfitting, early stopping was used as a regularization method because of the effectiveness and simplicity [44]. Training and test errors were calculated after every iteration. If the test error increased over a certain number of iterations, the running calculation was stopped. The parameters of the ANN are summarized in Table 4 and remain unchanged for the following investigations.

4. Results

To compare the predictive power of the presented machine learning models, the datasets were pre-processed, and features were extracted. Decisive features were chosen based on their correlation strength and combined to gain the minimum prediction error. Subsequently, several classification tasks were performed with varying amounts of production and cycling data as input.

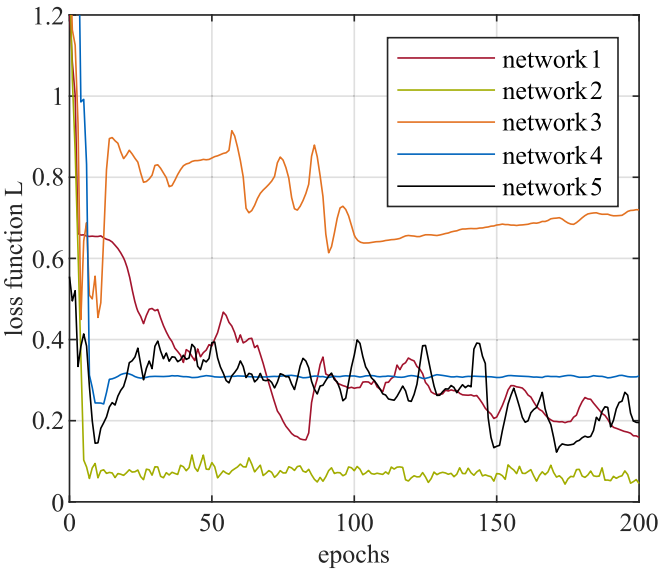

Fig. 3. Comparison of five network architectures. The number of epochs defines the repetitions in which the learning algorithm runs through the entire training dataset. Number and structure of the hidden layers varied for the respective nets and are listed in Table 3. The respective loss functions were determined using the classification task, presented in Section 4.3. A further evaluation using the prediction task can be found in the Supplementary Fig. 1.

Table 3
Structure of the compared network architectures. The selected "network 2", which is depicted in Fig. 2, is highlighted in gray.

Layer	1	2	3	4	5	6	7	8
Network 1	40	35	30	25	20	15	10	5
Network 2	40	32	24	16	8	-	-	-
Network 3	40	30	20	10	-	-	-	-
Network 4	40	20	-	-	-	-	-	-
Network 5	20	10	-	-	-	-	-	-

4.1. Data analysis

Initially, the database, which is necessary for an accurate prediction, was identified. Since the complete dataset is too complex to be analyzed in the regression, features were extracted, which served as input for the machine learning models. An overview of all examined features, ordered by correlation strength, can be found in the Supplementary Material. A separation can be made into features extracted from the electrochemical impedance spectroscopy (resistance) and features extracted from the battery test system (voltage and current). Furthermore, the features can be divided according to their respective process step: wetting, formation, or cycling. Features obtained from cycling are most commonly used in the literature. This is because most studies aim to determine the

Table 4
Summary of the specifications of the selected ANN.

Parameter	Specification
Network architecture	Five hidden layers (40 – 32 – 24 – 16 – 8 neurons)
Activation function	RELU-function
Optimizer	AdaMax
Learning rate	Adaptive learning rate (starting at 0.1)
Regularization method	Early-Stopping

remaining useful life by using commercially available cells. Hence, information on cell production is not included, which limits the potential for early cycle life prediction. Regarding the cycle life prediction during initial cycling, Severson et al. and Zhu et al. have reported a number of promising features that were included in this work [21,22]. However, formation and wetting features have not been reported so far. Several features were therefore extracted from production data and examined regarding their suitability for early cycle life prediction and classification.

Table 5 shows the two features from the respective sources with the highest correlations. Correlation coefficients were calculated using Eq. (1). Δ indicates the difference, while the variance describes the second momentum of the distribution. The features generated from the EIS and formation data show only a weak correlation. However, the features extracted from the cycling have the highest correlations due to the data obtained from multiple charge and discharge cycles. For all aging features, a relatively constant and high correlation was achieved when using a reference cycle number of 20. The number resulted from a sensitivity analysis, which is shown in Fig 4.

The discharge capacity was chosen as a feature for the sensitivity analysis because it has the highest correlation Successively, the difference in discharge capacity of two distinct cycles n and k was determined and the percentage error was calculated using the linear regression model. The percentage error is high when two cycles (n-k) with similar cycle numbers are used, because of the respective small amount of data. After approx. 50 cycles, a significant increase in the percentage error is observed. This effect is due to the two regeneration cycles with a lower C-Rate of C/10 and C/2, respectively (see Table 2). The lower C-rate results in an increased capacity, which significantly decreases the quality of the linear regression model. The small yellow section in the middle of the graph is explained by the regeneration cycles, as the cells partially recover, and the capacity is higher at the 1C cycles afterwards. The second section at approx. 75 cycles and the increase of the percentage error in the upper right corner is attributable to the strong degradation of the cells. Since the capacity of cells with a small amount of electrolyte start decreasing early, the cells deviate strongly from a linear degradation (see Fig. 1). Looking at the inset, a significantly lower percentage error is obtained if cycle 1 is chosen as a reference. This is due to the regeneration cycles at the start of the measurement. In this case, the percentage error decreases in the following cycles. The short rate capability test, in the beginning, provides valuable information to the linear regression model since without the regeneration cycles worse results are obtained. Hence, the usage of cycle 1 as a reference for cycle k leads to an improved model performance. Further analysis on the required number of input cycles n is provided in the next section.

Table 5
Comparison of correlation values of exemplary features. Correlation coefficients were calculated between the respective feature and the cycle life using the information depicted in the parenthesis for each cell in the dataset. Features generated by the difference of two cycles are separated by a ",". A listing of all analyzed features is shown in the Supplementary Table A2. The reference cycle c_{ref} for the aging features is varied in the range of cycle 15 and cycle 25.

Feature	Pearson correlation
Wetting	
High frequency resistance (after wetting)	+ 0.14
Low frequency resistance (after wetting)	+ 0.11
Formation	
Difference discharge capacity (formation)	-0.40
Variance Discharge difference (formation)	+0.39
Cycling	
Δ Discharge capacity (cycle 1, c_{ref})	-0.92
Variance discharge capacity (cycle 1 - c_{ref})	-0.89

4.2. Model comparison based on the regression

To compare the performance of the linear regression model with the ANN, the test errors using varying numbers of features were evaluated. Fig. 5 shows the prediction error for the feature with the highest correlation to analyze the number of input cycles needed. The reference cycle corresponds to cycle n in Fig. 4, with cycle k=1 remains constant. For each data point, the respective model was re-trained with randomly selected datasets. Subsequently, the resulting percentage errors of five distinct test runs were averaged and the respective standard deviations calculated. One run involves training the model with 20 random cells and testing it with nine random cells. The specifications for the used ANN are listed in Table 4. Using only a few cycles as input, the percentage error as well as the standard deviation is high for both, the linear regression and the ANN. For the linear regression, the percentage error rises for few reference cycles and then decreases continuously until a minimum is reached at reference cycle 19. A similar trend is observed for the ANN. However, the decrease is faster and fluctuates more for a small number of reference cycles.

Despite the fluctuations, the percentage error of the ANN is smaller than the percentage error of the linear regression model and reaches the first minimum at cycle 16. The fluctuations are due to the non-linearity of the ANN. Each additional cycle trains the network, resulting in a different weighting. For an increasing number of reference cycles, the percentage error increases for the linear regression. This is due to the non-linear aging behavior of the battery cells, which is difficult to describe using a linear regression model.

Yang et al. differentiated between linear and non-linear aging, depending on the degradation effect [45]. Linear aging arises from additional SEI formation in cycling due to cracking of the SEI [46]. This process consumes electrolyte as well as cyclable lithium, reducing the cell capacity. If a critical amount of electrolyte is depleted or the electrolyte quantity is insufficient, ion conductivity through the pores of the separator diminishes [47]. This results in lithium plating and causes non-linear aging of the cells, especially for smaller amounts of electrolyte [24]. Thus, the degradation of the cells is non-linear and a non-linear model like the ANNs is superior in modeling the behavior. A cycle number of 20 is chosen for further evaluation and comparison of the models since at this point both models converge steadily and show a small test error.

Table 6 shows an excerpt of the selected feature combinations. Test errors of the predicting models with different feature combinations were obtained using five test runs, each with re-trained models. Looking at the linear regression model, using only the feature “Δ discharge capacity” results in an average test error of 14.3%. Similar results were obtained with other high-correlation features like the variance of the discharge capacity, which exhibits a test error of 14.5%. The best result was gained using the combination of three input features, consisting of the difference, the variance, and the kurtosis of the discharge capacity until cycle 20. Using this feature combination, a test error of 13.9% was achieved. These results are in good agreement with Severson et al. who identified the variance of the discharge capacity as the feature with the highest correlation [22]. The high correlation of the other two features can be explained by the capacity losses during initial cycling. The losses are attributable to the electrolyte consumption and drying out of the insufficiently filled cells.

The combination of nine features did not improve the results due to the high dimensionality. Thus, it is essential to consider which features are combined in the linear regression. For the ANN, the combination of features has less influence on the test error, since the values are within the respective standard deviation for combinations with up to nine features. Using a few features slightly reduced the test errors in comparison to the linear regression. The improvement becomes apparent when more features are used. In contrast to the linear regression model, the lowest test error (10.1%) of the ANN was obtained with 29 input features. These consist of nine features with a high or moderate

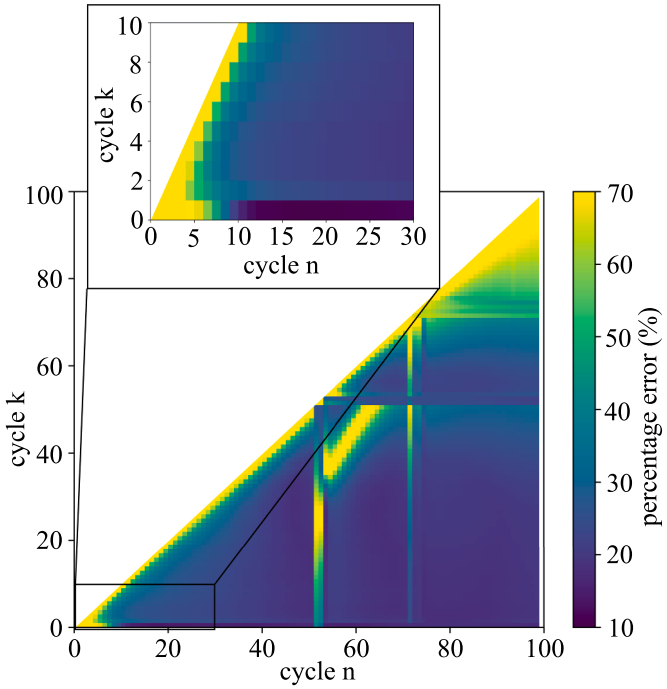

Fig. 4. Prediction error in dependence of two distinct cycles. The percentage errors are obtained with the input feature "Δ Discharge capacity" between cycle n and cycle k (n>k) using the linear regression model. The inset located below, displays an enlarged section of the full diagram. The percentage errors are color-coded from yellow to blue for high to low values. The artefacts at cycle k=1 and between cycle n=50 and n=70 are due to regeneration cycles at a lower C-Rate (see Table 2).

correlation to the cycle life and the discharge capacity of the first 20 cycles. However, for each combination, the test error of the ANN is lower than the linear regression model. A complete list of all features used and their respective correlations can be found in the Supplementary Table A2.

In summary, the ANN allows for a lower percentage error with a higher amount of input features than the linear regression model. Therefore, the ANN was used for the subsequent classification tasks. The discharge capacity and its second and third moments were identified as suitable features to predict the cycle life. Accordingly, manufacturers should consider these features initially when predicting cell quality. Since several cycles are required for an accurate prediction, it is examined in the following whether an early classification with production data is possible.

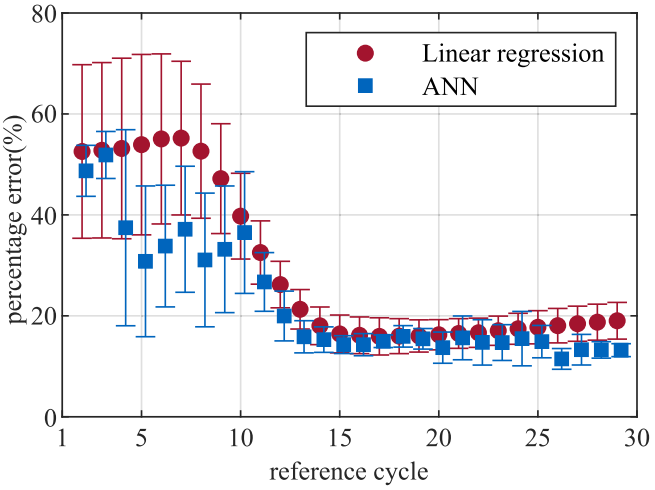

Fig. 5. Prediction error depending on the number of input cycles. The percentage errors are obtained using the input feature "Δ discharge capacity" between cycle one and a reference cycle. for each data point, 5 runs containing 9 test cells each were performed using a re-trained model. The resulting percentage errors were averaged, and the standard deviation of the runs was calculated.

4.3. Classification task

For the first classification task, the cells were divided into two different groups: A low cycle life group with a cycle life smaller than 250 cycles and a high lifetime group with a cycle life higher than 250 cycles. Using the ANN, a classification of the cells with a varying amount of input data was performed and the results were compared. The test results of the individual classifications are shown in Fig. 6a-d and a quantitative comparison in Table 7. For the first case (Fig. 6a), only data from EIS after wetting was used. Since the extracted EIS features showed a rather small correlation (see Table 5), a raw data approach was chosen, and the complete dataset from wetting was provided unfiltered into the neural network. In the second case (Fig. 6b), the data from the formation process was added. The data was also provided unfiltered since the features showed a medium correlation strength (see Table 5). In the third and fourth case (Figs. 6c & 6d), the dataset was augmented with

Table 6
Comparison of test errors for the two prediction models using an increasing number of features. The feature information for the combinations is shown in the Supplementary Table A2.

Number of features	Test error linear regression	Test error ANN
1	14.3 (± 1.4)%	12.9 (± 2.6)%
3	13.9 (± 2.3)%	13.1 (± 3.4)%
9	18.7 (± 3.3)%	13.5 (± 2.5)%
29	-	10.1 (± 1.1)%

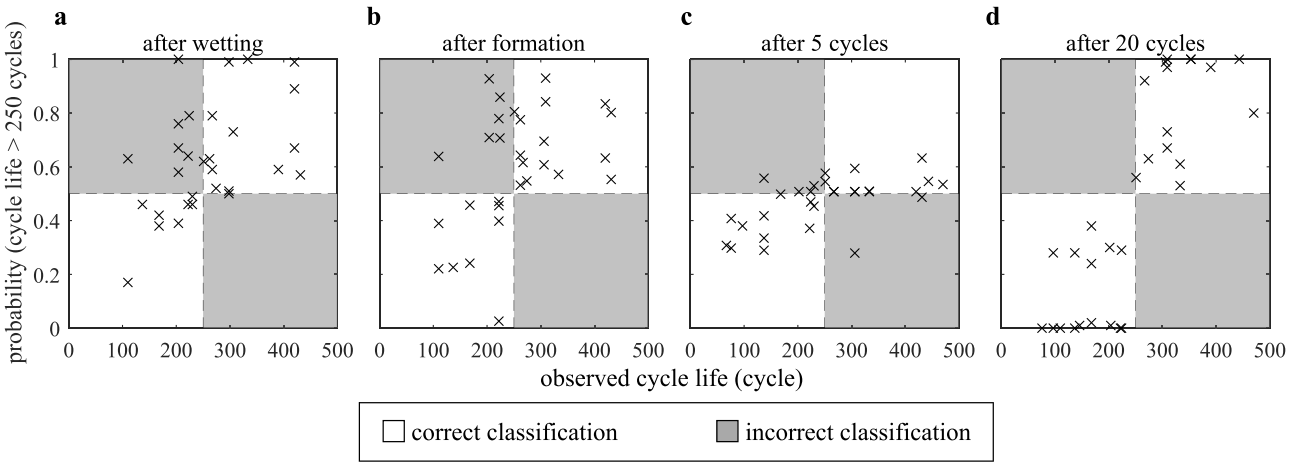

Fig. 6. Classification into two groups with high and low cycle life. (a-d) The probability reflects the certainty of the ANN in classifying the individual cells in the high cycle life group (cycle life > 250 cycles). A value close to 1 indicates a high probability that the cell has a cycle life greater than 250 cycles, while a value close to 0 indicates a high probability of obtaining a cycle life less than 250. A value close to 0.5 reflects an uncertainty in the prediction. The results of the classification task a-c were obtained with a varying amount of input data. for each graph, 5 test runs were performed with the ANN being re-trained each time. The false positive (upper left) and false negative (bottom right) quadrants are highlighted in dark gray. The average classification accuracies based on a number of 20 test runs are shown in Table 7.

the values from the discharge capacity of the first 5 and 20 cycles, respectively.

To evaluate the reliability and the performance of the model, the calculations were repeated five times using random training and test data in each run. Next to the classification itself, the probabilities were analyzed to determine the certainty of the model. The probabilities indicated how certain the ANN classifies the cells and allowed a more precise analysis of the performance. A probability close to 1 indicated that the cell is very likely to belong to the high lifetime group and a probability close to 0 indicated that the cell is more likely to belong to the low lifetime group. At a value close to 0.5, the ANN was not able to make a clear distinction between the high and low lifetime groups. Hence, plotting the probability over the lifetime as done in Figs. 6a-d, a classification in the lower left and the upper right quadrant was correct; a classification in one of the other two quadrants was incorrect. The incorrect quadrants were highlighted in gray. The mean classification accuracies are summarized Table 7.

Fig. 6a shows the classification results for case 1 (EIS data from wetting). For most cells, the ANN returned a probability close to 0.5, which indicated a rather uncertain classification. Nevertheless, most of the cells were classified correctly, resulting in an accuracy of 80%. Accuracy is defined as the correct classifications divided by the total number of classifications. Considering that no currents were applied so far, the predominantly correct classification indicates the high relevance of the EIS data. Furthermore, incorrect classifications occurred in the area of false positives only. This means that cells classified below 250 cycles actually have a cycle life of less than 250 cycles. The implications for battery production are further discussed in Section 5.

Adding the formation data increased the accuracy of the classification to 88%. As seen in Fig. 6b, a slight shift in probability away from 0.5 is visible for the classified cells. Similar to the prior classification, no false negatives occurred. Although the results were improved by adding the formation data, a significant number of cells were still misclassified.

Fig. 6c shows the classification results using the production data and the datasets of the first 5 cycles of the subsequent cycling. For the first time, false positives occurred and a shift of the probabilities closer to 0.5 is visible. Consequently, the classification accuracy decreases to 82%, which is mainly due to the increasing C-Rates during initial cycling. This is consistent with the observations in Fig. 4, where a minimum of 10 cycles is required to improve the prediction result.

Adding the datasets of the first 20 cycles of the subsequent cycling improved the classification significantly to an accuracy of 97%. Misclassifications were greatly reduced and only one cell with a cycle life close to the 250 cycles threshold was incorrectly classified. Considering the observed cycle lives of many cells being close to the 250 cycles threshold, the classification using the enhanced dataset shows excellent results. The increasing probabilities indicate a high reliability of the model.

Next to the classification into two groups, the cells were classified in three different cycle life groups for a closer examination. The three groups were chosen in regard to a comparable number of cells per group. The first group has a cycle life of less than 150 cycles, the second in the range of 150 - 300 cycles, and the third greater than 300 cycles. The results of the three-way classification are summarized in Table 7. In contrast to the classification in two groups, the model with the formation and wetting data as input had the lowest classification accuracy of 64%. Using only the wetting data resulted in a slightly higher accuracy of 67%. Adding the datasets of the first 20 cycles improved the accuracy significantly. However, the classification in two groups achieved a higher accuracy for all databases due to the limited number of training cells.

Table 7
Accuracy for classification tasks in two and three groups, respectively. Classification accuracies were calculated with a different set of input data and a number of 20 test runs, using a re-trained ANN for each run.

Data	Accuracy 2 groups	Accuracy 3 groups
After wetting	80%	67%
Formation	88%	64%
5 cycles	81%	69%
20 cycles	97%	89%

4.4. Grading task

In addition to the classification tasks, a cycle life prediction was performed with a subsequent grading dependent on the predicted cycle life. The ANN was used to predict the cycle life and grade the cells in four different quality groups as an example. The classification algorithm lost a considerable degree of accuracy when the number of classification groups increased (see Table 7). This is due to the decreasing ratio of training cells to classification possibilities. Since an early prediction is favorable, only formation and wetting data were used for the first grading. The data set was identical to the second case in Section 4.3.

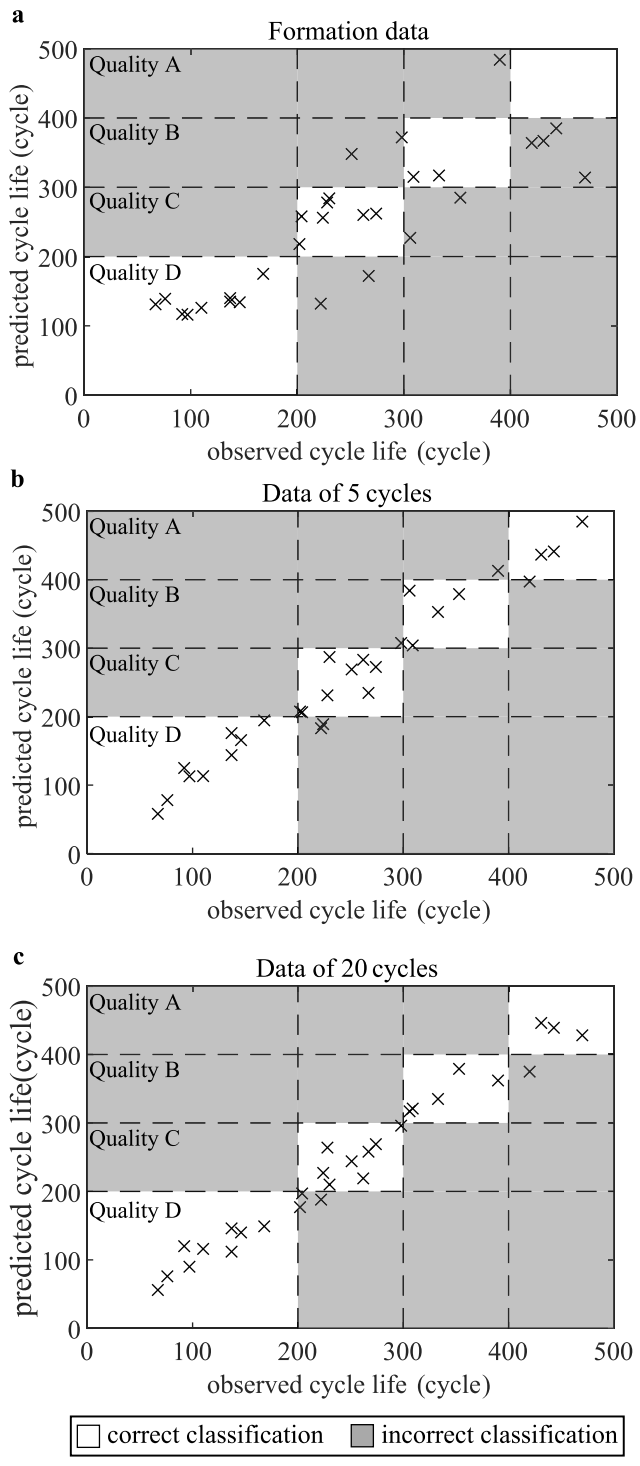

Fig. 7. Classification into quality grades. Predicted cycle life over observed cycle life and classification in quality groups with formation data (a), cycling data of the first 5 cycles (b), and cycling data of the first 20 cycles (c). for each graph, five test runs were performed with the ANN being re-trained each time. If the cycle life prediction is accurate, the predicted cell is located close to the diagonal. Quality grades were defined exemplarily every 100 cycles, starting at 200 cycles, and a letter A-D was assigned for each grade.

Subsequently, the cycling data of the first 20 cycles was added, and a second grading was performed. The results are shown in Figs. 7a-c. Here the range of low cycle life cells (Quality D) spanned from 0 to 200 cycles. The other quality groups C – A were defined exemplarily in increasing steps of 100 cycles. Cells that have a predicted cycle life in the range of the observed cycle life group were correctly graded (white area). Incorrectly graded cells are placed in the gray area. The best prediction result is an arrangement of data points on the diagonal of the graph.

By using the formation and wetting data only, all cells with a cycle life less than 200 cycles were correctly graded at Quality D. However, at higher cycle lives, the prediction accuracy decreases to an overall accuracy of 62%. Fig 7a shows that all the cells with a cycle life greater than 400 cycles were misplaced at Quality B instead of Quality A. Hence, the data base after formation seems to be insufficient for an exact grading into multiple quality groups, but cells with low cycle life were reliably detected.

Adding the datasets of the first 5 cycles enabled a more accurate prediction for cells with a higher cycle life. The previously strongly scattered cells were arranged closely along the ideal diagonal. As seen in Fig 7b., misclassification still occurred in different quality grades, resulting in an overall accuracy of 83%. This is consistent with the uncertainty of the regression model, when using a few numbers of cycles (compare Fig 4). Nevertheless, in comparison to the classification into two groups, the results can be improved using datasets from cycling.

Fig. 7c shows the grading results when the datasets of the first 20 cycles are added. Again, the difference between observed and predicted cycle life was small. Misclassifications occurred rarely and only for cells with a cycle life near the boundaries between two quality grades, resulting in an overall accuracy of 86%. In all gradings, the classification accuracy was smaller than in the classification task (see Fig. 6). This is due to the presence of four groups instead of two and the strictly defined thresholds. However, all misclassified cells are located very close to the respective boundary. Consequently, an accurate grading using the ANN was possible, which enables the application of data-driven early quality classification in the production of LIBs.

5. Discussion

A major challenge in the production of LIBs is ensuring the cell quality. The conventional quality measures such as aging are time-consuming and costly [6]. Therefore, the potential of the data-driven predictive quality models for industrial battery production as well as the impact on the process chain are the scope of the following discussion.

5.1. Early detection of process deviations

As shown in Table 1, the amount of electrolyte was intentionally varied in the experiments to obtain process deviations. An insufficient amount of electrolyte results in an incomplete wetting state of the cell. This leads to significant problems in the subsequent formation, as SEI cannot be formed homogeneously on all particles of the anode active material [48]. The resulting inhomogeneous SEI can lead to strong layer thickness fluctuations, which possibly induces partial layer detachments [49]. Furthermore, an insufficient electrolyte quantity result in the cells drying out during cycling, which has a negative effect on the capacity and cycle life [50]. Although the neural network was not given any information about the amount of electrolyte, it was possible to classify the majority of cells with a reduced cycle life correctly, using only impedance data from wetting and formation data (see Figs. 6a,b & Fig. 7a). In conventional production lines, the depicted process deviations are most likely apparent in the aging or EoL-test, since there were no significant variations in the capacities of the cells observable after the formation (see Table 1). Since aging takes up to 3 weeks [9], if the process deviations are detected late, it may result in the production of defective cells during a period of process instability. The delayed detection leads to high scrap costs. This demonstrates the great potential of data-driven analysis to detect process defects already during wetting and formation in comparison with time-consuming quality assurance processes.

5.2. Increase in throughput

Besides analyzing process deviations, data-driven analysis helps to detect defective cells at an early stage and thus increases the production throughput. The later a defective cell is detected, the greater are the associated costs due to further refinement and the blocking of plant capacity. Especially the latter point is a critical aspect in cell finishing as the processes are time-intensive and cells require single processing stations (e.g. a test channel during the self-discharge measurement). This leads to a reduction in throughput and longer depreciation times and costs. It was shown that neural networks help to determine the quality of LIBs, in terms of cycle life, before the time- and resource-intensive aging step. Information from the wetting and the formation is hereby sufficient for a first quality classification (see Fig. 6). Although some cells were misclassified (20%), only a few false negatives occurred (<2%). Cells classified as defective are indeed defective and can be regarded as inferior or scrap. These cells can be rejected without further refinement, which results in increased processing capacities for higher quality cells and thus an improvement of the overall throughput.

5.3. Extended data basis for the quality determination

A classification into two distinct groups is preferred when trying to detect cells with inferior quality that have to be regarded as scrap [51]. Minor defects in the production of LIBs do not necessarily cause the complete failure of a cell, but rather reduce the cycle life or charging capability. However, homogeneity of quality is a decisive factor for the customer, particularly in the increasingly important application areas of electromobility. A single inferior cell significantly affects the performance of the entire battery pack and makes an early replacement necessary [52]. Therefore, manufacturers must ensure high quality within production and are obliged to specify a minimum service life or a minimum number of achievable cycles. Since manufacturers cannot cover all use cases, cycle life can only be guaranteed if standardized environmental and operational conditions are applied. This frequently translates into test procedures using full charge/discharge cycles at a fixed C-Rate and temperature to determine the cycle life of a cell. With the presented prediction and classification methods, the manufacturer can exploit the production data and achieve early quality assurance without time-consuming cycling. Predicting early cycle life is therefore a different challenge than determining the exact RUL, which is often used in dynamic battery operation in the application [12].

From a production point of view, a classification into multiple quality grades is advantageous. The underlying principle is that cells with low quality can be additionally refined or sold as lower graded goods (e.g. second grade). By using measurement data from the wetting and formation process, an early classification into quality grades “A-D” was performed (see Fig. 7a). Here, almost all cells with a low service life were correctly assigned, but cells with a high service life were not. The addition of subsequently cycling data from the first 20 charge-discharge cycles at 1C, which corresponds to a cycling time of two days, resulted in significantly better classification. Only a few cells (all with cycle lives close to the defined classification limits) were misclassified. Manufacturers can use the data-driven analysis to supplement the quality determination from aging and the EoL-test to obtain an improved quality determination.

5.4. Alternative process routes

As mentioned, LIBs are aged for up to three weeks due to the high-quality requirements. However, since no refining is performed and plant capacity during aging is a key factor in increasing the overall throughput, the process step has great potential for streamlining. It was shown by Severson et al. that an accurate classification into two or more quality grades is possible after only a few charge-discharge cycles [22]. An accuracy of 97% was achieved for classification into two groups, whereas wrong classifications occurred only within 10 cycles of the threshold (see Figs. 6c, 6d, and Table 7). Analyzing the classification probability, the ANN correctly grouped many cells using less than 20 cycles. If an accurate classification is possible after a few cycles, a short cycling period instead of time-intensive aging could be favorable in terms of processing costs and throughput. The use of process and cell data from previous process steps in combination with a neural network and cycling data could allow for the prediction of the cycle life in real-time. As soon as a cell is reliably grouped into a quality grade during the cycling period, the cell can be sold according to the quality group. However, further research is needed to evaluate whether the cyclization approach performs better than the conventional aging, regarding the quality determination, and if this method is economically viable.

6. Conclusion

In this work, data-driven machine learning approaches were used for an early quality prediction and classification in battery production. Linear regression models and artificial neural networks (ANNs) were compared regarding their prediction accuracy using diverse datasets of 29 NMC111/graphite pouch cells. The favorable ANN achieved a minimum test error of 10.1% for a total of 29 input features. Nevertheless, the linear regression shows comparable test errors of approx. 13% when only a few input features are used.

In a second step, the preferable ANN was selected for classification into lifetime groups according to the cycle life of the cells. The best classification model obtained an accuracy of 97% for classification into two cycle life groups. By using the measurement data after wetting (EIS data) and after formation (EIS & formation data), a classification accuracy of 80% and 88% was achieved, respectively. Since there were almost no false negatives in all classifications, the reliable detection of defective cells was indicated. Finally, the capability of data-driven neural networks was demonstrated by predicting the cells’ cycle life and subsequently grading into quality groups. Although the neural network had no information on cell chemistry or degradation mechanisms, a high degree of accuracy was achieved by extracting features from electrical and electrochemical analysis.

The findings may be used in the future to detect defective cells at an early stage in lithium-ion battery production, increasing throughput and enhancing overall quality. Process errors can be detected quickly, and the process flow can adapt based on the quality prediction. Further research will focus on the increase of the prediction accuracy in wetting and formation as well as the quantification of the cost reduction through cycle-based aging.

CRediT authorship contribution statement

Sandro Stock: Conceptualization, Methodology, Investigation, Visualization, Formal analysis, Data curation, Validation, Writing – original draft, Writing – review & editing. **Sebastian Pohlmann:** Methodology, Investigation, Software, Validation, Visualization. **Florian J. Günter:** Formal analysis, Data curation, Validation, Writing – review & editing, Supervision, Project administration, Funding acquisition. **Lucas Hille:** Investigation, Writing – review & editing. **Jan Hagemeister:** Investigation, Writing – review & editing. **Gunther Reinhart:** Supervision, Project administration, Funding acquisition.

Declaration of Competing Interest

The authors declare that they have no known competing financial interests or personal relationships that could have appeared to influence the work reported in this paper.

Acknowledgments

This work was primarily supported by the project “OptiPro” (grant number: 03XP0364B) as part of the competence cluster “InZePro” by the

Federal Ministry of Education and Research in Germany (BMBF). Moreover, the authors are grateful for the use of cell data obtained in the project “Cell-Fill” (grant number 03XP0237B) within the competence cluster “ProZell2” by the Federal Ministry of Education and Research in Germany (BMBF).

Supplementary materials

Supplementary material associated with this article can be found, in the online version, at doi:10.1016/j.est.2022.104144.

References

[1] R.J. Brodd, Batteries, Introduction. Batteries for Sustainability – Selected Entries from the Encyclopedia of Sustainability Science and Technology, Springer Science +Business Media, New York, 2012, https://doi.org/10.1007/978-1-4614-5791-6.
[2] A. Kwade, W. Haselrieder, R. Leithoff, A. Modlinger, F. Dietrich, K. Droeder, Current status and challenges for automotive battery production technologies, Nat. Energy 3 (2018) 290–300, https://doi.org/10.1038/s41560-018-0130-3.
[3] M. Wolter, g. Fauser, C. Bretthauer, M.A. Roscher, End-of-Line Testing and Formation Process in Li-Ion Battery Assembly Lines. International Multi-Conference on Systems, Signals & Devices, IEEE, 2012, pp. 1–3, https://doi.org/10.1109/SSD.2012.6198092.
[4] S.J. An, J. Li, Z. Du, C. Daniel, D.L. Wood, Fast formation cycling for lithium ion batteries, J. Power Sources 342 (2017) 846–852, https://doi.org/10.1016/j.jpowsour.2017.01.011.
[5] R. Korthauer, Handbuch Lithium-Ionen-Batterien, Springer Berlin Heidelberg, Berlin, Heidelberg, 2013.
[6] D.L. Wood, J. Li, S.J. An, Formation challenges of lithium-ion battery manufacturing, Joule 3 (2019) 2884–2888, https://doi.org/10.1016/j.joule.2019.11.002.
[7] X. Yue, J. Kiely, S. Ghauri, M. Kauer, M. Bellanger, D. Gibson, A successive approximation method to precisely measure leakage current of the rechargeable lithium coin battery, J. Energy Storage 13 (2017) 442–446, https://doi.org/10.1016/j.est.2017.08.006.
[8] X. Sun, Y. An, L. Geng, X. Zhang, K. Wang, J. Yin, Q. Huo, T. Wei, X. Zhang, Y. Ma, Leakage current and self-discharge in lithium-ion capacitor, J. Electroanal. Chem. 850 (2019), 113386, https://doi.org/10.1016/j.jelechem.2019.113386.
[9] D.L. Wood, J. Li, C. Daniel, Prospects for reducing the processing cost of lithium ion batteries, J. Power Sources 275 (2015) 234–242, https://doi.org/10.1016/j.jpowsour.2014.11.019.
[10] D. Krüpper, K. Kuhlmann, S. Wolf, Pieper Cornelius, G. Xu, J. Ahmed, The Future of Battery Production for Electric Vehicles, BCG analysis, 2018, 1. https://www.bcg.com/de-de/publications/2018/future-battery-production-electric-vehicles (accessed 22 March 2021).
[11] X.-S. Si, W. Wang, C.-H. Hu, D.-H. Zhou, Remaining useful life estimation – A review on the statistical data driven approaches, Eur. J. Oper. Res. 213 (2011) 1–14, https://doi.org/10.1016/j.ejor.2010.11.018.
[12] L. Wu, X. Fu, Y. Guan, Review of the remaining useful life prognostics of vehicle lithium-ion batteries using data-driven methodologies, Appl. Sci. 6 (2016) 166, https://doi.org/10.3390/app6060166.
[13] A. Nuhic, T. Terzimehic, T. Soczka-Guth, M. Buchholz, K. Dietmayer, Health diagnosis and remaining useful life prognostics of lithium-ion batteries using data-driven methods, J. Power Sources 239 (2013) 680–688, https://doi.org/10.1016/j.jpowsour.2012.11.146.
[14] Q. Miao, L. Xie, H. Cui, W. Liang, M. Pecht, Remaining useful life prediction of lithium-ion battery with unscented particle filter technique, Microelectron. Reliab. 53 (2013) 805–810, https://doi.org/10.1016/j.microrel.2012.12.004.
[15] C. Hu, G. Jain, P. Tamirisa, T. Gorka, Method for estimating capacity and predicting remaining useful life of lithium-ion battery, Appl. Energy 126 (2014) 182–189, https://doi.org/10.1016/j.apenergy.2014.03.086.
[16] Y. Cheng, C. Lu, T. Li, L. Tao, Residual lifetime prediction for lithium-ion battery based on functional principal component analysis and Bayesian approach, Energy 90 (2015) 1983–1993, https://doi.org/10.1016/j.energy.2015.07.022.
[17] Y. Zhang, C.-Y. Wang, X. Tang, Cycling degradation of an automotive $LiFePO_4$ lithium-ion battery, J. Power Sources 196 (2011) 1513–1520, https://doi.org/10.1016/j.jpowsour.2010.08.070.
[18] J. Wu, C. Zhang, Z. Chen, An online method for lithium-ion battery remaining useful life estimation using importance sampling and neural networks, Appl. Energy 173 (2016) 134–140, https://doi.org/10.1016/j.apenergy.2016.04.057.
[19] S.S. Mansouri, P. Karvelis, G. Georgoulas, G. Nikolakopoulos, Remaining useful battery life prediction for UAVs based on machine learning, IFAC 50 (2017) 4727–4732, https://doi.org/10.1016/j.ifacol.2017.08.863.
[20] L. Ren, L. Zhao, S. Hong, S. Zhao, H. Wang, L. Zhang, Remaining useful life prediction for lithium-ion battery–A deep learning approach, IEEE Access (2018) 50587–50598, https://doi.org/10.1109/ACCESS.2018.2858856.
[21] S. Zhu, N. Zhao, J. Sha, Predicting battery life with early cyclic data by machine learning, Energy Storage (2019), https://doi.org/10.1002/est2.98.
[22] K.A. Severson, P.M. Attia, N. Jin, N. Perkins, B. Jiang, Z. Yang, M.H. Chen, M. Aykol, P.K. Herring, D. Fraggedakis, M.Z. Bazant, S.J. Harris, W.C. Chueh, R. D. Braatz, Data-driven prediction of battery cycle life before capacity degradation, Nat. Energy 4 (2019) 383–391, https://doi.org/10.1038/s41560-019-0356-8.
[23] G. Reinhart, T. Zeilinger, J. Kurfer, M. Westermeier, C. Thiemann, M. Glonegger, M. Wunderer, C. Tammer, M. Schweier, M. Heinz, Research and demonstration center for the production of large-area lithium-ion cells, in: G. Schuh, R. Neugebauer, E. Uhlmann (Eds.), Future Trends in Production Engineering, Springer Berlin Heidelberg, Berlin, Heidelberg, 2013, pp. 3–12, https://doi.org/10.1007/978-3-642-24491-9_1.
[24] F.J. Günter, C. Burgstaller, F. Konwitschny, G. Reinhart, Influence of the electrolyte quantity on lithium-ion cells, J. Electrochem. Soc. 166 (2019) A1709–A1714, https://doi.org/10.1149/2.0121910jes.
[25] F.J. Günter, R. Gilles, G. Reinhart, Introduction to electrochemical impedance spectroscopy as a measurement method for the wetting degree of lithium-ion cells, J. Electrochem. Soc. (2018) 165, https://doi.org/10.1149/2.0081814jes.
[26] J. Landesfeind, J. Hattendorff, A. Ehrl, W.A. Wall, H.A. Gasteiger, Tortuosity determination of battery electrodes and separators by impedance spectroscopy, J. Electrochem. Soc. 163 (2016) A1373–A1387, https://doi.org/10.1149/2.1141607jes.
[27] R. Bhagwat, M. Abdolahnejad, M. Moocarme, Applied Deep Learning With Keras: Solve complex Real-Life Problems With the Simplicity of Keras, Packt Publishing Ltd, 2019. ISBN: 978-1838555078.
[28] A. Ly, M. Marsman, E.-J. Wagenmakers, Analytic posteriors for Pearson’s correlation coefficient, Stat. Neerl. 72 (2018) 4–13, https://doi.org/10.1111/stan.12111.
[29] M. Kondo, C.-P. Bezemer, Y. Kamei, A.E. Hassan, O. Mizuno, The impact of feature reduction techniques on defect prediction models, Empir. Softw. Eng. 24 (2019) 1925–1963, https://doi.org/10.1007/s10664-018-9679-5.
[30] A.V. Joshi, Machine Learning and Artificial Intelligence. Machine Learning and Artificial Intelligence, 1st, Springer International Publishing, 2020, https://doi.org/10.1007/978-3-030.
[31] H. Zou, T. Hastie, Regularization and variable selection via the elastic net, J. R. Stat. Soc. 67 (2005) 301–320, https://doi.org/10.1111/j.1467-9868.2005.00503.x.
[32] Y. Shen, B. Han, E. Braverman, Stability of the elastic net estimator, J. Complex. 32 (2016) 20–39, https://doi.org/10.1016/j.jco.2015.07.002.
[33] A. Géron, Praxiseinstieg Machine Learning mit Scikit-Learn, Keras und TensorFlow: Konzepte, Tools und Techniken für intelligente Systeme, in: Aktuell zu Tensorflow 2, O’Reilly, Heidelberg, 2018, ISBN 978-3960090618.
[34] F. Zhang, T.L. Lai, B. Rajaratnam, N.R. Zhang, StanfordUniversity, Department of Statistics, Cross-validation and Regression Analysis in High-dimensional Sparse Linear Models, Stanford University, 2011.
[35] G. Rebala, A. Ravi, S. Churiwala, An Introduction to Machine Learning. An Introduction to Machine Learning, Springer Nature Switzerland AG, Cham, 2019, https://doi.org/10.1007/978-3-030-15729-6.
[36] J. Frochte, Maschinelles Lernen–Grundlagen und Algorithmen in Python. Maschinelles Lernen: Grundlagen und Algorithmen in Python, 2nd ed., Carl Hanser Verlag, München, 2019. ISBN: 978-3-446-45996-0.
[37] Y. Goldberg, G. Hirst, Neural Network Methods in Natural Language Processing. Neural Network Methods in Natural Language Processing 1st, 10, Morgan & Claypool Publishers, 2017, https://doi.org/10.2200/S00762ED1V01Y201703HLT037.
[38] Y. Wu, W. Li, Y. Wang, K. Zhang, Remaining useful life prediction of lithium-ion batteries using neural network and bat-based particle filter, IEEE Access 7 (2019) 54843–54854, https://doi.org/10.1109/ACCESS.2019.2913163.
[39] Z.-H. Wang, G.-J.Horng Hendrick, H.-T. Wu, G.-J. Jong, A prediction method for voltage and lifetime of lead–acid battery by using machine learning, Energy Explor. Exploit. 38 (2019) 310–329, https://doi.org/10.1177/0144598719881223.
[40] S. Ryu, J. Noh, H. Kim, Deep neural network based demand side short term load forecasting, Energies 3 (10) (2017), https://doi.org/10.3390/en10010003.
[41] O. Campesato, Artificial Intelligence, Machine Learning, and Deep Learning, Mercury Learning & Information. Artificial Intelligence, Machine Learning, and Deep Learning, Mercury Learning and Information LLC, 2020. ISBN: 978-1683924678.
[42] S. Zhang, X. Guo, X. Zhang, Modeling of back-propagation neural network based state-of-charge estimation for lithium-ion batteries with consideration of capacity attenuation, Adv. Electr. Comput. Eng. 19 (2019) 3–10, https://doi.org/10.4316/AECE.2019.03001.
[43] D.P. Kingma, J. Ba, Adam–A method for stochastic optimization, Conference for Learning Representations 3 (2015).

[44] I. Goodfellow, Y. Bengio, A. Courville, Deep Learning. Deep Learning (Adaptive Computation and Machine Learning series), The MIT Press, 2016. ISBN: 978-0262035613.
[45] X.-G. Yang, Y. Leng, G. Zhang, S. Ge, C.-Y. Wang, Modeling of lithium plating induced aging of lithium-ion batteries–Transition from linear to nonlinear aging, J. Power Sources 360 (2017) 28–40, https://doi.org/10.1016/j.jpowsour.2017.05.110.
[46] A. Wang, S. Kadam, H. Li, S. Shi, Y. Qi, Review on modeling of the anode solid electrolyte interphase (SEI) for lithium-ion batteries, NPJ Comput. Mater. 4 (2018), https://doi.org/10.1038/s41524-018-0064-0.
[47] K.G. Gallagher, S.E. Trask, C. Bauer, T. Woehrle, S.F. Lux, M. Tschech, P. Lamp, B. J. Polzin, S. Ha, B. Long, Q. Wu, W. Lu, D.W. Dees, A.N. Jansen, Optimizing areal capacities through understanding the limitations of lithium-ion electrodes, J. Electrochem. Soc. 163 (2016) A138–A149, https://doi.org/10.1149/2.0321602jes.
[48] S.J. An, J. Li, C. Daniel, D. Mohanty, S. Nagpure, D.L. Wood, The state of understanding of the lithium-ion-battery graphite solid electrolyte interphase (SEI) and its relationship to formation cycling, Carbon 105 (2016) 52–76, https://doi.org/10.1016/j.carbon.2016.04.008.
[49] L. Somerville, J. Bareño, S. Trask, P. Jennings, A. McGordon, C. Lyness, I. Bloom, The effect of charging rate on the graphite electrode of commercial lithium-ion cells–A post-mortem study, J. Power Sources 335 (2016) 189–196, https://doi.org/10.1016/j.jpowsour.2016.10.002.
[50] A. Wang, S. Kadam, H. Li, S. Shi, Y. Qi, Review on modeling of the anode solid electrolyte interphase (SEI) for lithium-ion batteries, NPJ Comput. Mater. 4 (2018), https://doi.org/10.1038/s41524-018-0064-0.
[51] J. Schnell, G. Reinhart, Quality management for battery production–A quality gate concept, Procedia CIRP 57 (2016) 568–573, https://doi.org/10.1016/j.procir.2016.11.098.
[52] L. Xie, D. Ren, L. Wang, Z. Chen, G. Tian, K. Amine, X. He, A facile approach to high precision detection of cell-to-cell variation for li-ion batteries, Sci. Rep. 10 (2020) 7182, https://doi.org/10.1038/s41598-020-64174-2.